Sigma Journal of Engineering and Natural Sciences
Web page info: https://sigma.yildiz.edu.tr
DOI: 10.14744/sigma.2023.00087

Research Article

# Machining of Ti–6Al–4V alloy by fiber laser: Determining the effects of parameters on surface roughness

**Şefika KASMAN[1,*], Burak BÜYÜKER[2], Sertan OZAN[2]**

[1]*Department of Mechanical Engineering, Dokuz Eylul University, Izmir, 35340, Türkiye*
[2]*Department of Mechanical Engineering, Yozgat Bozok University, Yozgat, 66000, Türkiye*

## ARTICLE INFO

*Article history*
Received: 19 July 2021
Revised: 10 August 2021
Accepted: 12 September 2021

**Keywords:**
Laser Engraving; Ti-6Al-4V; Surface Roughness; ANOVA

## ABSTRACT

The laser engraving process was used to make a gravure on the surface of Ti–6Al–4V alloy. The determinative effect of the laser beam was used to engrave the material on the interaction region using laser engraving parameters. Among the basic laser engraving parameters; scan speed, scan direction, and fill spacing were selected to determine the engraving character of Ti-6Al-4V alloy. The Taguchi L18 orthogonal array was used to set up an experimental layout to analyze the effects of laser engraving on surface roughness and engraving depth. The signal-to-noise ratios for both surface roughness and engraving depth were calculated using the experimental data and also, it was used to decide which factor combination represents the optimal process responses. Further, the analysis of variance was used to decide on the significance of parameters at a 95% confidence level. The results obtained from the analysis of variance revealed that scan speed and scan direction are the critical parameters as p- values are lower than 0.05 and affect the surface roughness by 53% and 19%, respectively. However, scan speed and scan direction affect the engraving depth by 64% and 10%, respectively.

**Cite this article as:** Kasman Ş, Büyüker B, Ozan S. Machining of Ti–6Al–4V alloy by fiber laser: Determining the effects of parameters on surface roughness. Sigma J Eng Nat Sci 2023;41(4):770–780.

## INTRODUCTION

Demand for the development of energy-saving machining processes is increasing in some industrial applications where cost is important. Manufacturing techniques, especially in precision machining applications involving complex geometries, require special cutting tool production techniques and tool materials, experience, and precise machines, so there could be difficulties depending on the chosen manufacturing method. Some industries use thermal energy-based precision machining applications particularly to make miniature grooves and/or details that could not be machined using tool-assisted machining methods [1, 2]. Besides, critical application techniques considering dimensional accuracy and surface tolerances are important factors in choosing between processing spectra. Laser-Assisted Machining (LAM), Electro Discharge Machining (EDM), and Wire Electro-Discharge Machining (WEDM) are commonly preferred

***Corresponding author.**
*E-mail address: sefika.kasman@deu.edu.tr

*This paper was recommended for publication in revised form by Regional Editor Chandramohan V.P.*

methods in precision machining methods compared to the conventional material removal methods to achieve the desired geometry using thermal energy [3]. The laser-assisted machining technique for removing material from the hard metal is a comparatively effective and prominent shaping technique because EDM and WEDM methods require metals to be electrically conductive. Material removal from hard materials is a critical issue for some geometries in precision applications to create a net shape in the desired surface profile. The predominant feature of the LAM is the absence of tool and tool-dependent defects (e.g. wear, breakage, and chatter) [4]. These features make the LAM a machining method for miniature gravures that could not be machined using tool-based methods. The laser beam is used for applications such as milling, drilling, marking, engraving, cutting, and sintering [3] in aerospace, automotive, biomedical, and electronics industries [5, 6] in the machining process of precision shapes on the workpieces. In particular, some materials that exhibit poor machinability [2, 4, 6] using conventional machining methods could be manufactured using LAM. Titanium alloys are in the groups of difficult-to-machine materials [6-10] using conventional machining techniques due to their high strength and hardness. Titanium alloys exhibit an excellent strength-to-weight ratio [8-10], low density, good corrosion resistance, low thermal conductivity, and high biocompatibility [5, 11-13]. Due to above mentioned inherent properties of titanium and its alloys, its usage as the engineering material in aerospace and automotive industries, biomaterials [9, 14, 15], and marine applications [10] has become widespread.

Laser engraving is a milling process used to evaporate the material with the thermal interaction between the laser beam and the metal. This thermal interaction is highly affected by beam scan speed, frequency, and power. The intensity of thermal interaction determines the amount of material vaporized in the interaction zone and the amount of liquid phase remaining after vaporization. These sequential cases ensure the material is removed from the interaction region layer by layer. The scan times or the numbers of material removal cases determine the milling depth. The material that evaporated per scan time determines the engraving depth, and the material that solidifies at the surface following evaporation characterizes the surface roughness. LAM is an effective machining technique for small biomedical devices and/or complex geometry in an engineering part. LAM techniques use a beam as a heat source and this heat source locally heats the material and then subsequently vaporizes from the contact area [16]. With the movement of the laser beam on the surface like a milling tool, the desired geometry is produced. According to the researchers, absence of cutting force and tool wear during the machining process, the machining productivity could be improved by 15%–50% [17, 18]. It also aids in to use of different machining strategies and flexibility in the production process [16]. Venkatesan et. al. [16] have studied the laser machining of hard-to-cut metals; they have concluded that LAM improves the machining performance of hard-to-machining metals when compared to the traditional machining process. Dandekar et. al. [19] have performed hybrid machining using LAM to develop the machining of Ti–6Al–4V alloy with decreased cutting energy and surface roughness. Rashid et. al. [20] studied the impact of laser power on the cutting force and heat in the machining process of the Ti-6Cr-5Mo-5V-4Al alloy; it was revealed that the power significantly influenced the cutting force compared to the cutting speed analyzed. Sun et. al. [21] performed a comparative study to analyze the reduction of cutting forces and chip formation when laser power is used as a process parameter. Dargusch et. al. [18] evaluated the performance of cutting tools with different coating types for machining titanium alloys.

The literature overview of LAM of Ti–6Al–4V alloy has shown that the studies on creating engraving or milling are limited. The present study focused on the application of engraving with laser milling parameters on Ti–6Al–4V alloy; and the process parameters of laser scan speed (SS), fill spacing (FS) and, laser beam scan direction (scan strategy, SD) were evaluated using surface roughness (SR) and engraving depth (D).

## MATERIALS AND METHODS

### Material

The rod sample with a 14 mm diameter of titanium alloy Grade 5: (Ti6Al4V) was used in the experimental studies. The chemical and mechanical properties of the Ti-6Al-4V alloy are given in Tables 1 and 2, respectively [22].

### Laser engraving process

A 50W Yb: Fiber Laser marking machine (see Figure 1) with a 1064 nm wavelength was used for laser engraving applications. A constant value of 160 mm was determined for the focal length on the processing surfaces. The

**Table 1.** Chemical composition of Ti-6Al-4V [wt. %] [22]

| Al | V | Fe | C | N | H | O | Ti |
|---|---|---|---|---|---|---|---|
| 5.5~ 6.8 | 3.5~ 4.5 | ≤0.3 | ≤0.08 | ≤0.05 | ≤0.015 | ≤0.2 | Bal. |

**Table 2.** Mechanical properties of Ti-6Al-4V [22]

| Elongation | Hardness | Tensile Strength | Yield Strength | Elastic Modulus | Fracture Toughness |
|---|---|---|---|---|---|
| [%] | [HV] | [MPa] | [MPa] | [GPa] | [MPa.m$^{1/2}$] |
| 13-16 | 300-400 | 900-1200 | 800-1100 | 110-140 | 33-110 |

engraving process was applied to the titanium alloy samples. The engraving test samples were put on an aluminum plate. The engraving area was determined to be a 10 x 10 mm$^2$ area and was scanned 20 times. It is well known that the parameters that exhibit a highly influential effect on surface roughness are scan speed, scan direction, and, fill spacing. The engraving process was analyzed by considering three main process control factors and changing levels are given in Table 3. The selected values for scan speed (SS), scan direction (SD), and, fill spacing (FS) were determined by the preliminary experiments for surface roughness (SR). The ranges for SS were determined to achieve higher engraving depth (D). In this context, the selected values for all the parameters were determined with the aim of achieving lower SR at higher D. Based on three control factors and their levels, a laser engraving strategy with the Taguchi method was executed. The L18 orthogonal layout was created to perform engraving experiments and analyze the data taken from the machined surfaces.

**Table 3.** Control factors and their levels

| Notation | Parameters | Levels | | |
|---|---|---|---|---|
| | | 1 | 2 | 3 |
| *FS* | Fill spacing (mm) | 0.02 | 0.04 | - |
| *SS* | Scan Speed (mm.s$^{-1}$) | 100 | 200 | 300 |
| *SD* | Scan Direction (°) | 45°/45° | 45°/90° | 90°/0° |

The average SR (Ra) and D were measured using a Mitutoyo SJ400 stylus-type profilometer and a linear height

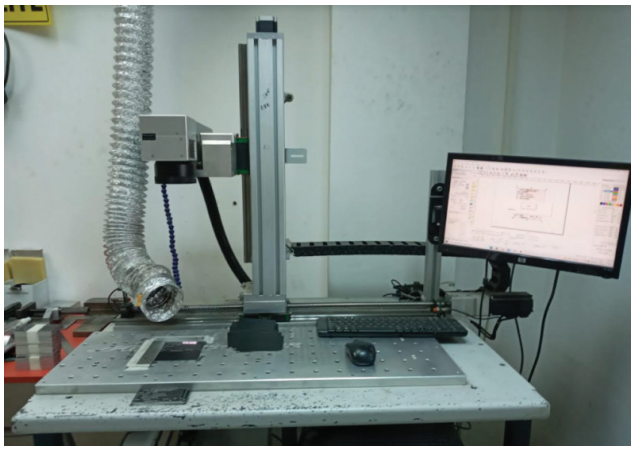

**Figure 1.** Laser engraving system.

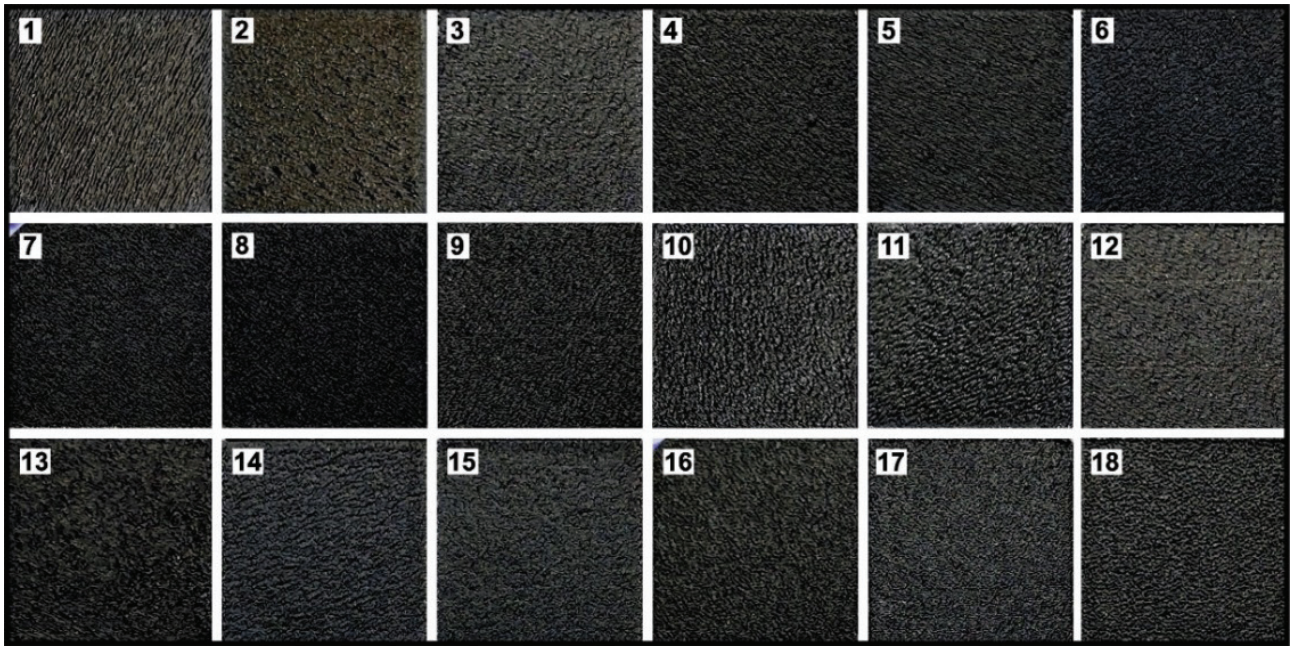


**Figure 2.** Laser-engraved surfaces by the test procedure.

gauge (Mitutoyo LH-600E BS-Type), respectively. The cut-off length and the sampling number for Ra were arranged as 0.8 mm and 5, respectively; and the calculated pin moving distance was 4 mm. Both SR and D measurements were repeated 2 times in each axis considering the axes of the rectangular field. For Ra, a region near the center of the rectangular field was determined as the measurement area. The laser-engraved surface of all the samples is given in Figure 2.

**Microstructural analysis**

The scan direction determines the laser machining strategy. The scan direction which greatly affects the surface roughness [23, 24], affects the macrostructure of the machined surface and the microstructures of a narrow area just below the machined surface [23, 24]. Therefore, the microstructural analyses were performed on the cross-section of the machined surface to determine the machining strategy's effect on the transition zone (between the machined surface and base metal). The standard metallographic procedures were performed on the machined surface's cross-section; the samples were etched using Kroll reagent for 60 s. The optical microscopy studies were performed on the etched surface. The hardness measurements were performed on the cross-sectioned surface that was located below the laser beam processed area. A hardness profile was created starting from craters formed from the vaporized and re-cast material. Micro-vickers hardness tester (Metkon MH-3) was used in the hardness measurements. The hardness trace was performed with a 50 g load for 10 s.

**Methodology of statistical analyses**

Determination of the smoothest surface roughness in the deepest cavity is a critical issue for the present study, and the research question is which machining strategy is the best alternative to reach the optimal SR and D. With this approach, the Taguchi method combined with the analysis of variance (ANOVA) was studied to specify the best engraving strategy. In case a process has more than one response and these responses affect the process at the same or different weight, the Taguchi optimization technique is the best solution to identify the unknown information [25]. The optimization procedure comprises the stages, namely determining the appropriate orthogonal array, determining of signal to noise ratio (S/N), predicting optimum process parameters and their levels, and ANOVA analysis.

## RESULTS AND DISCUSSIONS

Laser engraving was performed on the surface of titanium alloy test specimens to analyze and explain the impact of process variables on SR and D. The variables, namely SS, SD, and, FS were selected as process control factors. The effects of those control factors having different test values were analyzed using the Taguchi with L18 orthogonal array. The highest D and the lowest SR characterize a better engraving process. Therefore, the response characteristics should be the lowest SR and the highest D.

**Determining the Appropriate Orthogonal Array**

The control factors, SS at three levels, SD at three levels, and, FS at two levels, were used to determine the orthogonal array and perform laser engraving experiments. The degrees of freedom (DOF) of parameters were determined by the number of parameters. The interactions were neglected. Based on the total DOF value of each parameter, the L18 orthogonal array was chosen to perform the laser engraving tests. A total of eighteen laser engraving tests were performed to assign the combination of parameters giving the lowest SR at the highest D. The selected L18 orthogonal array is seen in Table 4.

**Calculation of Signal-to-Noise Ratio (S/N)**

The S/N ratio is used to assign the optimum level of control factors that describe the process and analyze the parameter variation [15], thus meaning that the calculation of the S/N ratio is the first stage of processing experimental data collected from the measurements on the surface of test samples processed using laser engraving process. The signal defines the desired value expected from the process and the noise is the undesired control factor that could not be controlled during the process [26]. The aim of the calculation of the S/N ratio is to reduce the variability [26]. The calculations in the S/N ratio are performed using one of three different performance characteristics - the higher the better, the smaller the better, and the nominal the better [26]. Therefore, the quality characteristics for process responses should be selected before the normalization process. For the present study, the smaller the better and the larger the better characteristics represent the SR and the D, respectively. The selection of the smaller the better characteristics for SR maximizes the S/N ratio [27-31], and the selection of the higher the better characteristics for D also, maximizes the S/N ratio. This approach makes it possible to deduce that two quality characteristics represent the laser engraving process. The quality characteristics representing the desired SR and D are given in Eq. 1 and Eq.2, respectively [32-34].

$$\eta = \frac{S}{N} = -10\log\left(\frac{1}{n}\sum_{i=1}^{n} Y_i^2\right) \quad (1)$$

$$\eta = \frac{S}{N} = -10\log\left(\frac{1}{n}\sum_{i=1}^{n} \frac{1}{Y_i^2}\right) \quad (2)$$

where $Y_i$ is the process response and n is the number of experiments.

The SR and D values seen in Table 4 correspond to the data measured from the laser-processed surface. The aim

of this process is to minimize the SR and maximize the D. Based on this aim, the S/N ratios for SR and D were calculated using Eq. 1 and Eq. 2, respectively. The calculated S/N ratios are given in Table 4.

**Determining of Optimum Level for Control Factors and Discussion**

The optimal combination of parameters for SR and D is specified by the mean of the S/N ratio for each level of the parameters. In addition, a graph depicted from the mean effect of the S/N ratios was utilized to specify the optimum control factors combination. The mean of the S/N ratio for SR and D is given in Tables 5 and 6. The main effect plots (data means), depicted according to measured data for SR and D, are seen in Figs. 3a and 3b, respectively. A larger S/N ratio is the scale of the robustness of an analyzed system, meaning that the variability created by the factors that control a process is minimized by the effect of reduced noise factors (uncontrollable factors).

The main effect plot of each control factor of the laser engraving process for SR and D is shown in Figs. 3a and 3b. The effect of the control factors on the SR and D is evaluated by considering the mean values of control factors for SR and D. Considering the SR values given in Figure 3a, the SR decreased while decreasing FS and SS. The SR value decreased between 45°/45° and 90°/0°. The highest value of the mean S/N ratio among all the levels seen in Table 5 indicates the optimal level (minimum SR for the investigated parameter. Based on this approach, the minimum SR could be achieved while FS was at 0.02 mm, SS was at 100 $mm.s^{-1}$ and SD was at 90°/0°. The optimal factor combination for SR was $FS_1SS_1SD_3$. The effect of factors on the D was analyzed using the mean data values of each factor given in Figure 3b. The plots show that the D decreased with increasing FS

**Table 4.** Taguchi orthogonal array L18 with responses (measured data for SR and D; S/N ratios for SR and D)

| *Exp. No* | *FS* | *SS* | *SD* | SR (µm) | $S/N_{SR}$ (dB) | D (µm) | $S/N_D$ (dB) |
|---|---|---|---|---|---|---|---|
| Exp.1 | 0.02 | 100 | 45°/45° | 16.61 | -24.41 | 248 | 47.89 |
| Exp.2 | 0.02 | 100 | 45°/90° | 14.38 | -23.16 | 152 | 43.64 |
| Exp.3 | 0.02 | 100 | 90°/0° | 9.81 | -19.83 | 177 | 44.96 |
| Exp.4 | 0.02 | 200 | 45°/45° | 15.12 | -23.59 | 126 | 42.01 |
| Exp.5 | 0.02 | 200 | 45°/90° | 14.46 | -23.2 | 112 | 40.98 |
| Exp.6 | 0.02 | 200 | 90°/0° | 14.71 | -23.35 | 92 | 39.28 |
| Exp.7 | 0.02 | 300 | 45°/45° | 16.62 | -24.41 | 77 | 37.73 |
| Exp.8 | 0.02 | 300 | 45°/90° | 19.42 | -25.76 | 48 | 33.62 |
| Exp.9 | 0.02 | 300 | 90°/0° | 17.11 | -24.67 | 32 | 30.10 |
| Exp.10 | 0.04 | 100 | 45°/45° | 15.14 | -23.6 | 86 | 38.69 |
| Exp.11 | 0.04 | 100 | 45°/90° | 16.01 | -24.09 | 118 | 41.44 |
| Exp.12 | 0.04 | 100 | 90°/0° | 10.79 | -20.66 | 109 | 40.75 |
| Exp.13 | 0.04 | 200 | 45°/45° | 15.44 | -23.77 | 82 | 38.28 |
| Exp.14 | 0.04 | 200 | 45°/90° | 15.53 | -23.82 | 67 | 36.52 |
| Exp.15 | 0.04 | 200 | 90°/0° | 13.14 | -22.37 | 58 | 35.27 |
| Exp.16 | 0.04 | 300 | 45°/45° | 20.98 | -26.44 | 64 | 36.12 |
| Exp.17 | 0.04 | 300 | 45°/90° | 18.58 | -25.38 | 37 | 31.36 |
| Exp.18 | 0.04 | 300 | 90°/0° | 19.86 | -25.96 | 18 | 25.11 |

**Table 5.** Main effects of $S/N_{SR}$

| Level | $S/N_{SR}$ | | |
|---|---|---|---|
| | *FS* | *SS* | *SD* |
| 1 | -23.60* | -22.62* | -24.37 |
| 2 | -24.01 | -23.35 | -24.24 |
| 3 | - | -25.44 | -22.81* |
| Rank | 3 | 1 | 2 |

*Optimal level

**Table 6.** Main effects of $S/N_D$

| Level | $S/N_D$ | | |
|---|---|---|---|
| | *FS* | *SS* | *SD* |
| 1 | 40.02* | 42.89* | 40.12* |
| 2 | 35.95 | 38.72 | 37.93 |
| 3 | - | 32.34 | 35.91 |
| Rank | 3 | 1 | 2 |

*Optimal level

**Table 7.** Optimal levels of each control factor considering the main effect of $S/N_{SR}$ and $S/N_D$

| Level | SR | D |
|---|---|---|
| FS | 0.02 | 0.02 |
| SS | 100 | 100 |
| SD | 90°/0° | 45°/45° |

and SS. Also, the effect of SD on the D indicates that the D value decreased between 45°/45° and 90°/0° as in SR. The maximum D could be achieved while FS was at 0.02 mm, SS was at 100 mm.s$^{-1}$ and SD was at 45°/45°. The optimal factor combination for D was $FS_1SS_1SD_1$. The optimal combination determined from the highest S/N ratios for SR and D is reported in Table 7. It is seen in Table 7 that the FS of 0.02 mm and SS of 100 mm.s$^{-1}$ are the optimal levels for both SR and D.

As for the optimal level for SS, there is a similarity between optimal SR and D. While the optimal level for SR was 100 mm.s$^{-1}$, the optimal level for D was 100 mm.s$^{-1}$, explaining that a decrease in SS increases D and decreases SR. The optimal level of SD was different for SR and D. The optimal level for SR and D was 90°/0° and 45°/45°, respectively. The optimal level of each control factor for SR and D was one of the engraving process conditions tested (Table 4-Exp. 3 and Exp. 1).

### Predicting Optimum SR and D

Prediction of optimal SR and D was performed by selecting the highest S/N ratio among the levels for each process parameter. A formula given in Eq. 3 [34] is used to determine the optimal SR and D [34].

$$\eta = \eta_m + \sum_{i=1}^{n}(\eta_i - \eta_m) \tag{3}$$

Using Eq. (3), the optimal SR, $S/N_{SR}$, D, $S/N_D$ are calculated as follows:

$$S/N_{SR} = FS_1 + SS_1 + SD_3 - 2.\eta_m$$
$$S/N_{SR} = -23.60 - 22.62 - 22.81 - 2.(-23.80) = -21.43\ dB$$
$$SR = FS_1 + SS_1 + SD_3 - 2.\eta_m$$
$$SR = 15.36 + 13.39 + 14.24 - 2.(15.76) = 11.47\ \mu m$$
$$S/N_D = FS_1 + SS_1 + SD_2 - 2.\eta_m$$
$$S/N_D = 40.02 + 42.89 + 40.12 - 2.(37.99) = 47.05\ dB$$
$$D = FS_1 + SS_1 + SD_2 - 2.\eta_m$$
$$D = 118.22 + 148.33 + 113.83 - 2.(94.61) = 191.2\ \mu m$$

The predicted S/N ratio and the mean value for SR were -21.43 dB and 11.47 µm, respectively. Also, the predicted S/N ratio and the mean value for D were 47.05 dB and 191.2 µm, respectively.

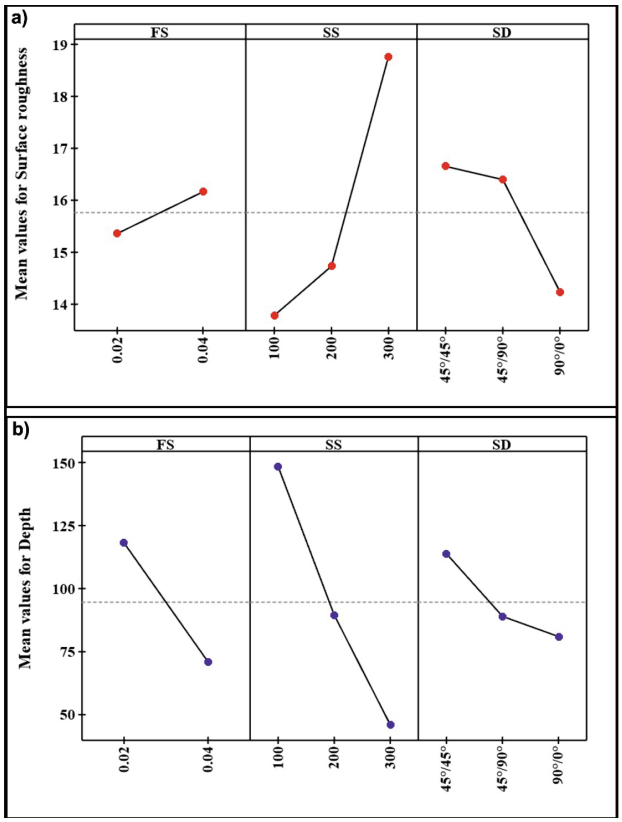


**Figure 3.** The graphs for mean values for SR (a) and D (b).

### Performing of ANOVA

Analysis of variance (ANOVA) was used as a statistical decision-making technique to determine the significance of the variables on SR and D. The statistical significance of the control factors was analyzed at a 95% confidence level (α=0.05) and the probability value (p-value) was used to decide about the significance of each variable on the SR and D. This means that if a p–value is less than 0.05, the relevant factor being investigated is significant. In addition, percentage contribution is used to explain the importance of factors on SR and D. The ANOVA for $S/N_{SR}$ is given in Table 8. According to the p–values given in Table 8, except the FS, SS and SD are statistically significant. The percentage effect of the parameters on SR was calculated in descending order SS (53%), SD (18.7%), and FS (1.6%). The results in the ANOVA analysis for D seen in Table 9 indicated that all the factors are statistically significant due to p–values less than 0.05, meaning that these parameters exhibit a significant effect on the D. The control factors, SS, FS and SD affect the D by 64%, 14.1%, and 10%, respectively.

### Hardness Measurements

The hardness profile starting from the re-cast layer towards the base metal for each engraved surface was obtained. Figure 4 shows the cross-section of the engraved surfaces. The hardness profile was created as a function of

**Table 8.** ANOVA results for $S/N_{SR}$ ratios

| Source | Process Parameters | | | | |
|---|---|---|---|---|---|
| | **FS** | **SS** | **SD** | **Error** | **Total** |
| *D.F.* | 1 | 2 | 2 | 12 | 17 |
| *Seq. SS* | 0.76 | 25.56 | 9.01 | 12.90 | 48.24 |
| *Adj. MS* | 0.76 | 12.78 | 4.50 | 1.075 | - |
| *p* | 0.415 | 0.01 | 0.042 | - | - |
| *Percentage Contribution (%)* | 1.6 | 53 | 18.7 | 26.7 | |

**Table 9.** ANOVA results for $S/N_D$ ratios

| Source | Process Parameters | | | | |
|---|---|---|---|---|---|
| | **FS** | **SS** | **SD** | **Error** | **Total** |
| *D.F.* | 1 | 2 | 2 | 12 | 17 |
| *Seq. SS* | 74.73 | 338.90 | 53.18 | 62.76 | 529.57 |
| *Adj. MS* | 74.73 | 169.45 | 26.59 | 5.23 | - |
| *p* | 0.003 | 0.000 | 0.025 | - | - |
| *Percentage Contribution (%)* | 14.1 | 64 | 10 | 11.9 | |

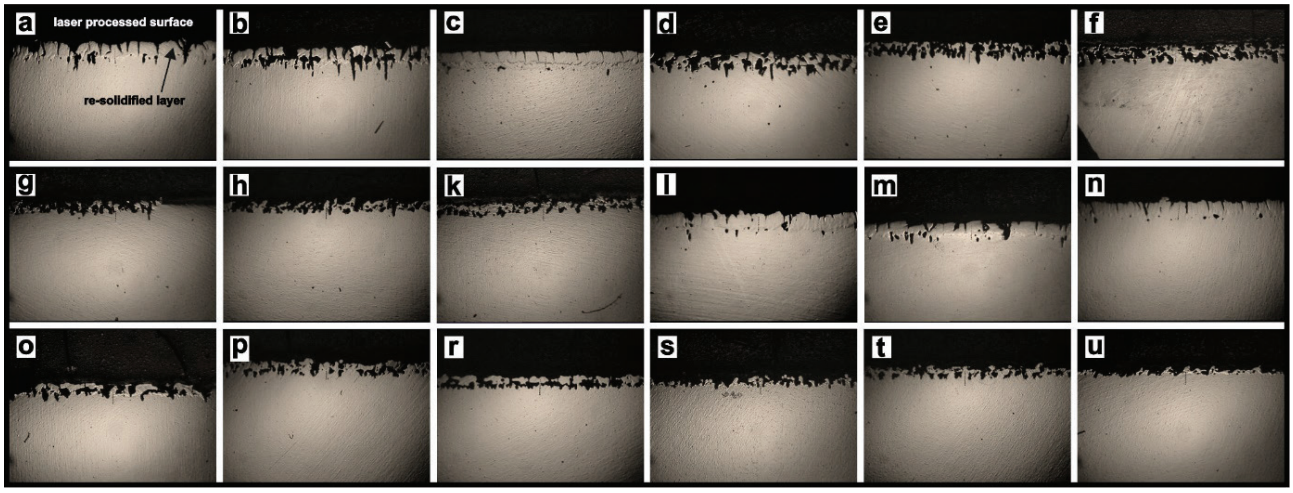


**Figure 4.** The processed (engraved) surface.

the distance and the distance between successive hardness traces was set to be 25 μm.

The results of the hardness measurements are given in Table 10 and Figure 5. The hardness of the base metal was measured to be between 302-326 HV 0.05. The highest hardness value among all the hardness values by means of distance was obtained with the process parameters of 0.02 mm FS, 100 mm.s$^{-1}$ SS and 45°/90° SD. The other highest hardness value at the re-cast layer was obtained with the process parameters of 0.04 mm FS, 200 mm.s$^{-1}$ SS and 45°/90° SD. These hardness values were measured to be 1283 and 1184 HV, respectively. Notably, a clear observation, drawn from the hardness values, is that the highest hardness values were obtained with the process parameters of 0.02 mm FS, 100 mm.s$^{-1}$ SS, and 45°/90° SD. It is clear that the hardness profile of each engraved sample (Figures 5a and 5b) exhibited similar trends except Exp. 2.

Laser-assisted machining methods are controlled by initial laser power (P, W), machined area (A, mm$^2$), beam spot diameter (D, mm), and scan speed (mm.s$^{-1}$). The relevant equations are given in Eq. 4 [24, 35].

$$t = \frac{D}{SS} \qquad E_v = \frac{P.D}{A.SS} \tag{4}$$

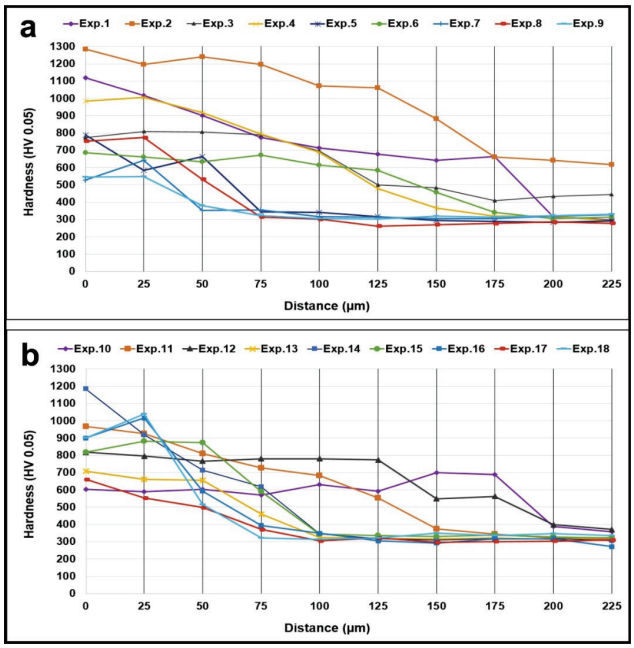


**Figure 5.** Hardness profiles as a function of distance starting from the re-cast layer.

where $E_v$ is the volume energy density (J/mm$^2$), t is the interaction time between laser beam and metal [24, 35]. The laser beam diameter and scan speed determine the interaction time. It is well known that for a constant beam diameter and initial laser power, any increase in interaction time between laser beam and metal increases the volume energy density. In this study, the laser beam diameter, initial laser power, and machining area are kept to be constant; therefore, the scan speed determines the volume energy density. The highest hardness value depending on the distance was obtained when the volume energy density was at the highest value which was obtained with the lowest scan speed. An increase in volume energy density increases the amount of vaporized metal at the interaction area, resulting in a rough surface profile caused by deep cavities behind. This leads to a harder re-cast layer on the laser-processed surface. It is well known that the re-cast layer consists of many craters at different depths and widths. Those craters determine the surface profiles of laser processed surface.

The surface profile of the re-cast layer is affected by the laser machining strategy (scan direction). The rough surface is seen in Figure 6a; this surface was obtained when the FS, SS and SD were set to be 0.02 mm, 100 mm.s$^{-1}$ and 45°/90°, respectively. It was revealed that the re-cast layer was consisted of two different regions, namely craters and subsurface layer (Figures. 6a-f). One of these regions, namely subsurface layer was found to be located under the craters; it was solidified slower than the other region. Besides slower solidification rate, subsurface layer exhibited different characteristics originating from the hardness value and microstructural evolution.

**Table 10.** Hardness values as a function of distance starting from the re-cast layer

| Exp. | Factors | | | Distance/Hardness values (HV 0.05) | | | | | | | | | |
|---|---|---|---|---|---|---|---|---|---|---|---|---|---|
| **No** | **FS** | **SS** | **SD** | **0** | **25** | **50** | **75** | **100** | **125** | **150** | **175** | **200** | **225** |
| **1** | 0,02 | 100 | 45°/45° | 1119 | 1017 | 900 | 773 | 713 | 677 | 643 | 665 | 317 | 298 |
| **2** | 0,02 | 100 | 45°/90° | 1283 | 1197 | 1239 | 1197 | 1072 | 1060 | 883 | 660 | 643 | 617 |
| **3** | 0,02 | 100 | 90°/0° | 773 | 808 | 806 | 788 | 695 | 501 | 483 | 409 | 435 | 444 |
| **4** | 0,02 | 200 | 45°/45° | 985 | 1006 | 918 | 794 | 689 | 480 | 365 | 319 | 320 | 291 |
| **5** | 0,02 | 200 | 45°/90° | 788 | 584 | 665 | 345 | 341 | 317 | 294 | 289 | 283 | 292 |
| **6** | 0,02 | 200 | 90°/0° | 686 | 661 | 633 | 672 | 613 | 584 | 456 | 340 | 306 | 313 |
| **7** | 0,02 | 300 | 45°/45° | 528 | 643 | 353 | 356 | 317 | 315 | 305 | 306 | 320 | 327 |
| **8** | 0,02 | 300 | 45°/90° | 753 | 773 | 532 | 315 | 302 | 262 | 270 | 277 | 286 | 278 |
| **9** | 0,02 | 300 | 90°/0° | 544 | 549 | 379 | 321 | 306 | 303 | 319 | 313 | 321 | 329 |
| **10** | 0,04 | 100 | 45°/45° | 603 | 589 | 603 | 570 | 631 | 593 | 701 | 689 | 388 | 359 |
| **11** | 0,04 | 100 | 45°/90° | 967 | 927 | 809 | 726 | 683 | 553 | 374 | 344 | 322 | 315 |
| **12** | 0,04 | 100 | 90°/0° | 818 | 795 | 766 | 781 | 780 | 773 | 549 | 562 | 399 | 371 |
| **13** | 0,04 | 200 | 45°/45° | 707 | 660 | 655 | 460 | 325 | 319 | 317 | 321 | 315 | 325 |
| **14** | 0,04 | 200 | 45°/90° | 1184 | 918 | 714 | 618 | 345 | 319 | 309 | 319 | 317 | 306 |
| **15** | 0,04 | 200 | 90°/0° | 818 | 883 | 874 | 589 | 345 | 335 | 329 | 339 | 327 | 321 |
| **16** | 0,04 | 300 | 45°/45° | 900 | 1016 | 593 | 394 | 349 | 305 | 293 | 317 | 317 | 271 |
| **17** | 0,04 | 300 | 45°/90° | 660 | 553 | 498 | 371 | 305 | 321 | 296 | 301 | 303 | 310 |
| **18** | 0,04 | 300 | 90°/0° | 900 | 1038 | 516 | 322 | 315 | 323 | 349 | 335 | 347 | 337 |

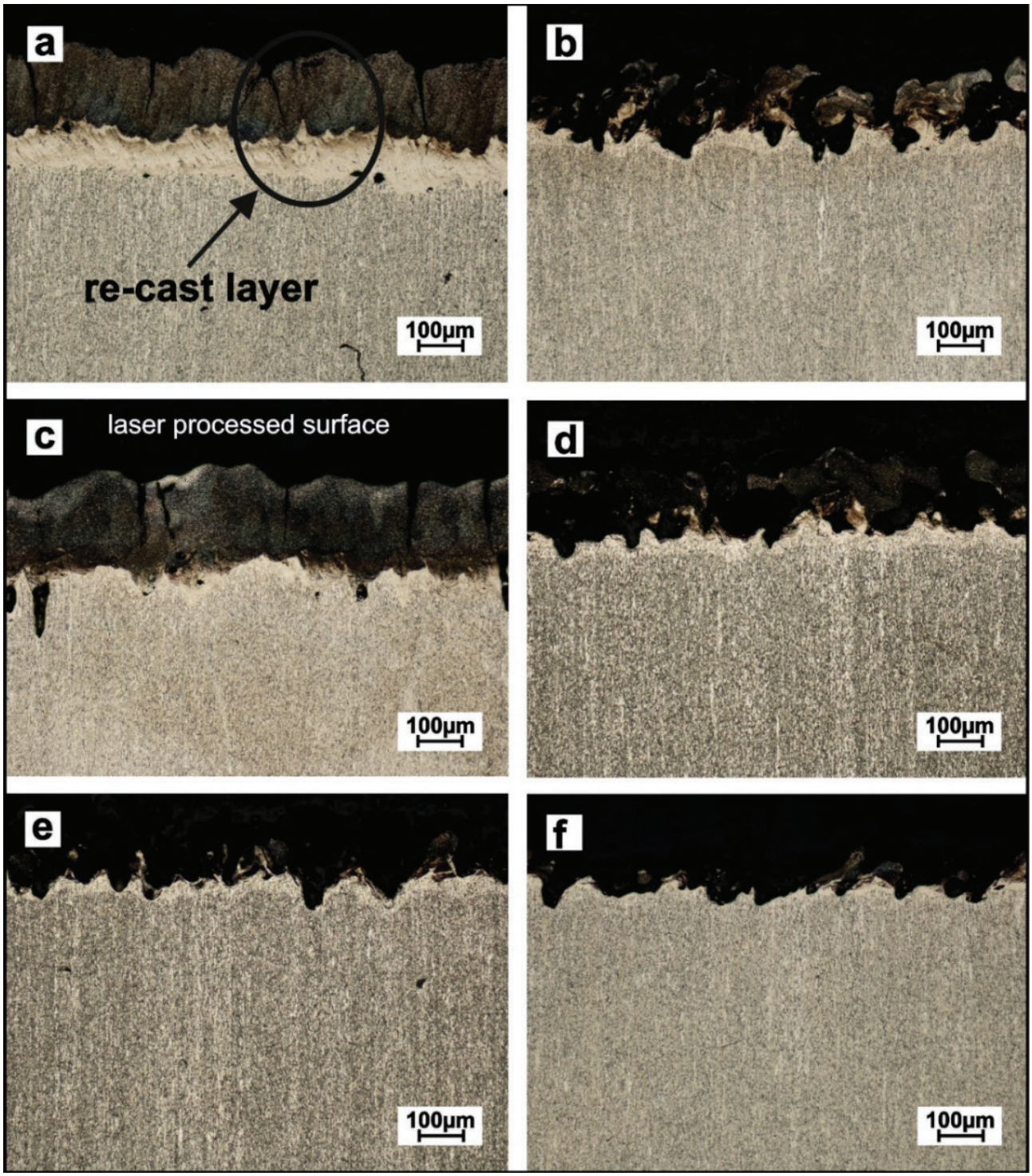


**Figure 6.** Surface profiles and re-cast layer after the laser engraving process.

The lowest thickness value of the subsurface layer among six re-cast layers is seen in Figure 6f. This microstructure image was taken from the specimen, engraved with the machining condition of 0.04 mm FS, 300 mm.s$^{-1}$ SS and 45°/90° SD. When the engraved specimens, seen in Figs. 6a and 6f, are compared to each other, it was concluded that FS and SS were effective in characterizing the re-cast layer. A similar re-cast layer given in Figure 6a is seen in Figure 6c, as well. The difference between machining conditions is FS and SD. Those two re-cast layers were obtained using SS of 100 mm.s$^{-1}$. Any decrease in SS led to a higher volume energy density, meaning that higher engraving depth and deeper interaction zone.

## CONCLUSIONS

The laser engraving process was employed on Ti6Al4V alloy using a 50W fiber laser. The effects of parameters were analyzed by the laser beam-titanium alloy metal interaction; and the result of this interaction was assessed using characteristic process responses, namely surface roughness (SR) and engraving depth (D). A L18 orthogonal array was used to analyze the three laser milling process parameters with different levels. The following conclusions are drawn:

a) Considering the selected process parameters, it was seen that the interaction between the laser beam and Ti-6Al-4V alloy managed SR and D.
b) The optimal level of each process parameter for SR considering the highest S/N ratio was stated as $FS_1SS_1SD_3$. The percentage effect of the parameters on SR, ranked in decreasing order, was SS (53%) > SD (18.7%) > FS (1.6%).
c) The optimum values for engraving depth considering the highest S/N ratio was the first level of FS, SS, and SD which was stated as $FS_1SS_1SD_1$. The parameters, namely SS, FS, and SD affect the D by 64%, 14.1% and, 10% respectively.
d) The FS affects SR and D by ~2% and 14%, respectively. It was concluded that the effectiveness of the fill spacing on SR is quite small. The selected levels for FS indicate that they do not make a significant difference.
e) The results obtained from the ANOVA analysis revealed that the scan speed was highly effective on both SR and D.
f) The highest hardness of the re-cast layer was measured to be 1283 HV; and it was obtained with the process parameters of 0.02 mm FS, 100 $mm.s^{-1}$ SS, and 45°/90° SD.

## AUTHORSHIP CONTRIBUTIONS

Authors equally contributed to this work.

## DATA AVAILABILITY STATEMENT

The authors confirm that the data that supports the findings of this study are available within the article. Raw data that support the finding of this study are available from the corresponding author, upon reasonable request.

## CONFLICT OF INTEREST

The author declared no potential conflicts of interest with respect to the research, authorship, and/or publication of this article.

## ETHICS

There are no ethical issues with the publication of this manuscript.

## REFERENCES

[1] Singh R, Alberts MJ, Melkote SN. Characterization and prediction of the heat-affected zone in a laser-assisted mechanical micromachining process. Int J Mach Tools Manuf 2008;48:994–1004. [CrossRef]
[2] Melkote S, Kumar M, Hashimoto F, Lahoti G. Laser assisted micro-milling of hard-to-machine materials. CIRP Ann Manuf Technol 2009;58:45–48. [CrossRef]
[3] Dubey AK, Yadava V. Laser beam machining - A review. Int J Mach Tools Manuf 2008;48:609–628. [CrossRef]
[4] Gilbert T, Krstic VD, Zak G. Machining of aluminum nitride with ultra-violet and near-infrared Nd: YAG lasers. J Mater Process Technol 2007;189:409–417. [CrossRef]
[5] Veiga C, Devim JP, Loureiro AJR. Properties and applications of titanium alloys: a brief review. Rev Adv Mater Sci 2012;32:133–148.
[6] Ahmed W, Elhissi A, Jackson MJ, Ahmed E. 2 - Precision machining of medical devices. In: Davim JP (editor). The Design and Manufacture of Medical Devices. Cambridge: Woodhead Publishing; 2012. p. 59–113. [CrossRef]
[7] Niknam SA, Khettabi R, Songmene V. Machinability and machining of titanium alloys: A review. In: Davim JP, editor. Machining of Titanium Alloys. Berlin: Springer-Verlag Berlin Heidelberg; 2014. p. 1–30. [CrossRef]
[8] Rahman M, Wang ZG, Wong YS. A review on high-speed machining of titanium alloys. JSME Int J C-Mech Sy 2006;49:11–20. [CrossRef]
[9] Veiga C, Davim JP, Loureiro AJR. Review on machinability of titanium alloys: the process perspective. Rev Adv Mater Sci 2013;34:148–164.
[10] Masood I. Sustainable machining for titanium alloy Ti-6Al-4V. In: Motyka M, Ziaja W, Sieniawsk J (editors). Titanium Alloys-Novel Aspects of Their Manufacturing and Processing. London: IntechOpen; 2019. p. 1–15. [CrossRef]
[11] de Viteri VS, Fuentes E. Titanium and titanium alloys as biomaterials. In: Gegner J (editor). Tribology-Fundamentals and Advancements. London: IntechOpen; 2013. p. 155–181. [CrossRef]
[12] Kumar A, Misra RDK. 3.4 - 3D-printed titanium alloys for orthopedic applications. In: Froes FH, Qian M (editors). Titanium in Medical and Dental Applications. Cambridge: Woodhead Publishing; 2018. p. 251–275. [CrossRef]
[13] Li YH, Yang C, Zhao HD, Qu SG, Li XQ, Li YY. New developments of Ti-Based alloys for biomedical applications. Materials 2014;7:1709–1800. [CrossRef]
[14] Hourmand M, Sarhan AAD, Sayuti M, Hamdi M. A Comprehensive review on machining of titanium alloys. Arabian J Sci Eng 2021;46:7087–7123. [CrossRef]

[15] Arrazola PJ, Garay A, Iriarte LM, Armendia M, Marya S, Le Maitre F. Machinability of titanium alloys (Ti6Al4V and Ti555.3). J Mater Process Technol 2009;209:2223–2230. [CrossRef]

[16] Venkatesan K, Ramanujam R, Kuppan P. Laser assisted machining of difficult to cut materials: research opportunities and future directions - A comprehensive review. In: Xavior MA, Yarlagadda P, (editors). 12th Global Congress on Manufacturing and Management, 2014. p. 1626–1636. [CrossRef]

[17] Norazlan MW, Mohid Z, Rahim EA. Laser assisted machining of titanium alloys. Mater Sci Forum 2013;763:91–106. [CrossRef]

[18] Dargusch MS, Sivarupan T, Bermingham M, Rashid RAR, Palanisamy S, Sun S. Challenges in laser-assisted milling of titanium alloys. Int J Extreme Manuf 2021;3:015001. [CrossRef]

[19] Dandekar CR, Shin YC, Barnes J. Machinability improvement of titanium alloy (Ti-6Al-4V) via LAM and hybrid machining. Int J Mach Tools Manuf 2010;50:174–182. [CrossRef]

[20] Rahman Rashid RA, Sun S, Wang G, Dargusch MS. The effect of laser power on the machinability of the Ti-6Cr-5Mo-5V-4Al beta titanium alloy during laser assisted machining. Int J Mach Tools Manuf 2012;63:41–43. [CrossRef]

[21] Sun S, Harris J, Durandet Y, Brandt M. Effect of laser beam on machining of titanium alloys. Pacific International Conference on Applications of Lasers and Optics 2008. p. 44–49. [CrossRef]

[22] Liu ZQ, Xu JY, Han S, Chen M. A coupling method of response surfaces (CRSM) for cutting parameters optimization in machining titanium alloy under minimum quantity lubrication (MQL) condition. Int J Precis Eng Manuf 2013;14:693–702. [CrossRef]

[23] Kasman S. Impact of parameters on the process response: A Taguchi orthogonal analysis for laser engraving. Measurement 2013;46:2577–2584. [CrossRef]

[24] Kasman S, Saklakoglu IE. The effect of process parameters on the surface form of laser engraved H13 tool steel. Kov Mater-Metal Mater 2013;51:317–325. [CrossRef]

[25] Ciftci I, Gokce H. Optimisation of cutting tool and cutting parameters in machining of molybdenum alloys through the Taguchi method. J Fac Eng Arch Gazi Univ 2019;34:201–213. [CrossRef]

[26] Kosaraju S, Venu Gopal A, Popuri BB. Taguchi analysis on cutting forces and temperature in turning titanium Ti-6Al-4V. Int J Mech Ind Eng 2012;1:55–59. [CrossRef]

[27] Akkus H, Yaka H. Experimental and statistical investigation of the effect of cutting parameters on surface roughness, vibration and energy consumption in machining of titanium 6Al-4V ELI (grade 5) alloy. Measurement 2021;167:108465. [CrossRef]

[28] Yaka H, Demir H, Gok A. Optimization of the cutting parameters affecting the surface roughness on free form surfaces. Sigma J Eng Nat Sci 2017;35:323–331.

[29] Kam M. Effects of deep cryogenic treatment on machinability, hardness and microstructure in dry turning process of tempered steels. Proc Inst Mech Eng E: J Process Mech Eng 2021;235:927–936. [CrossRef]

[30] Kam M, Demirtas M. Analysis of tool vibration and surface roughness during turning process of tempered steel samples using Taguchi method. Proc Inst Mech Eng E: J Process Mech Eng 2021;235:1429–1438. [CrossRef]

[31] Kam M, Seremet M. Experimental investigation of the effect of machinability on surface quality and vibration in hard turning of hardened AISI 4140 steels using ceramic cutting tools. Proc Inst Mech Eng E: J Process Mech Eng 2021;235:1565–1574. [CrossRef]

[32] Deresse NC, Deshpande V, Taifa IWR. Experimental investigation of the effects of process parameters on material removal rate using Taguchi method in external cylindrical grinding operation. Eng Sci Technol Int J 2020;23:405–420. [CrossRef]

[33] Ishfaq K, Zahoor S, Khan SA, Rehman M, Alfaify A, Anwar S. Minimizing the corner errors (top and bottom) at optimized cutting rate and surface finish during WEDM of Al6061. Eng Sci Technol Int J 2021;24:1027–1041. [CrossRef]

[34] Nain SS, Garg D, Kumar S. Investigation for obtaining the optimal solution for improving the performance of WEDM of super alloy Udimet-L605 using particle swarm optimization. Eng Sci Technol Int J 2018;21:261–273. [CrossRef]

[35] Romoli L. Flattening of surface roughness in ultrashort pulsed laser micro-milling. Precis Eng 2018;51:331–337. [CrossRef]